RNA (2000), *6*:220–232. Cambridge University Press. Printed in the USA.

Calculation of the relative geometry of tRNAs in the ribosome from directed hydroxyl-radical probing data

SIMPSON JOSEPH,[1,3] MICHELLE L. WHIRL,[2] DERRICK KONDO,[2] HARRY F. NOLLER,[1] and RUSS B. ALTMAN[2]

[1]Center for Molecular Biology of RNA, Sinsheimer Laboratories, University of California, Santa Cruz, California 95064, USA
[2]Stanford Medical Informatics, Stanford University, 251 Campus Drive, MSOB X-215, Stanford, California 94305-5479, USA

ABSTRACT

The many interactions of tRNA with the ribosome are fundamental to protein synthesis. During the peptidyl transferase reaction, the acceptor ends of the aminoacyl and peptidyl tRNAs must be in close proximity to allow peptide bond formation, and their respective anticodons must base pair simultaneously with adjacent trinucleotide codons on the mRNA. The two tRNAs in this state can be arranged in two nonequivalent general configurations called the R and S orientations, many versions of which have been proposed for the geometry of tRNAs in the ribosome. Here, we report the combined use of computational analysis and tethered hydroxyl-radical probing to constrain their arrangement. We used Fe(II) tethered to the 5′ end of anticodon stem-loop analogs (ASLs) of tRNA and to the 5′ end of deacylated $tRNA^{Phe}$ to generate hydroxyl radicals that probe proximal positions in the backbone of adjacent tRNAs in the 70S ribosome. We inferred probe-target distances from the resulting RNA strand cleavage intensities and used these to calculate the mutual arrangement of A-site and P-site tRNAs in the ribosome, using three different structure estimation algorithms. The two tRNAs are constrained to the S configuration with an angle of about 45° between the respective planes of the molecules. The terminal phosphates of 3′CCA are separated by 23 Å when using the tRNA crystal conformations, and the anticodon arms of the two tRNAs are sufficiently close to interact with adjacent codons in mRNA.

Keywords: ASL; computational model; structural conformation; tRNA

INTRODUCTION

Transfer RNAs (tRNAs) are the substrates used by ribosomes for synthesizing proteins. To understand the mechanism of translation at the molecular level, it is essential to understand how tRNAs interact with the ribosome (Rheinberger et al., 1981; Grajevskaja et al., 1982; Kirillov et al., 1983; Lill et al., 1984). The anticodon arm of P-site tRNA interacts with mRNA in the vicinity of the cleft formed by the platform and the head of the 30S subunit (Lake, 1980; Gornicki et al., 1984). The acceptor arms of A-site and P-site tRNAs interact with the peptidyl transferase center, which lies close to the base of the central protuberance of the 50S subunit (Ofengand, 1980; Olson et al., 1982; Wower et al., 1989). During peptide bond formation, the CCA-3′ termini of A-site and P-site tRNAs must be proximal to allow peptidyl transfer, while their anticodons interact with adjacent codons on mRNA (Fairclough & Cantor, 1979a; Matzke et al., 1980).

Several models have been proposed for the arrangement of A-site and P-site tRNAs in the ribosome based on stereochemical considerations (Fuller & Hodgson, 1967; Woese, 1970; Rich, 1974; Sundaralingam et al., 1975; Lake, 1977; Spirin & Lim, 1986; McDonald & Rein, 1987; Prabahakaran & Harvey, 1989; Nagano et al., 1991; Easterwood et al., 1994), fluorescence resonance energy transfer (FRET) (Johnson et al., 1982; Paulsen et al., 1983), crosslinking studies (Ofengand, 1980, Ofengand et al., 1981, 1986; Wower et al., 1989, 1993; Lim et al., 1992; Brimacombe et al., 1993; Spirin et al., 1993; Brimacombe, 1995; Mueller et al., 1997; Nagano & Nagano, 1997), chemical footprinting (Stern et al., 1988; Noller et al., 1990), cryoelectron microscopy (Agrawal et al., 1996; Stark et al., 1997a; Mal-

Reprint requests to: Russ B. Altman, Stanford Medical Informatics, Stanford University, 251 Campus Drive, MSOB X-215, Stanford, California 94305-5479, USA; e-mail: altman@SMI.Stanford.edu.
[3]Present address: Department of Chemistry and Biochemistry, University of California San Diego, La Jolla, California 92093, USA.

hotra et al., 1998), and other methods (Spirin, 1983; Smith & Yarus, 1989; Wagenknecht et al., 1989; Nierhaus et al., 1998). Most of these models can be assigned to either the R (Rich, 1974) or S (Sundaralingam et al., 1975) orientations. In the R orientation, the T loop of A-site tRNA faces the D loop of P-site tRNA, whereas in the S orientation, the D loop of A-site tRNA faces the T loop of P-site tRNA (Lim et al., 1992). The choice between these two orientations has important functional implications. In this study, we used Fe(II) tethered to anticodon stem-loop analogs (ASLs) of tRNA or to the 5′ end of full-length tRNA to probe directly the arrangement of tRNAs in the 70S ribosome. We constructed two sets of defined complexes. First, we formed ribosomal complexes having $tRNA_f^{Met}[^{32}P]pCp$ in the P site and either Fe(II)-ASLs or Fe(II)-$tRNA^{Phe}$ in the A site. The second set of complexes contained either Fe(II)-ASLs or Fe(II)-$tRNA^{Phe}$ in the P site and deacylated $tRNA^{Lys}[^{32}P]pCp$ in the A site. Hydroxyl radical formation was initiated and sites of cleavage in $tRNA_f^{Met}[^{32}P]pCp$ and $tRNA^{Lys}[^{32}P]pCp$ were identified by gel electrophoresis. The hydroxyl radical cleavage data were used to obtain distance constraints from which the relative orientation of the two tRNAs was calculated. These distance constraints were derived from calibration experiments reported previously (Joseph et al., 1997), and assume that stronger cleavage patterns (as measured by gel intensity) corresponded to closer interactions. We evaluated the sensitivity of the resulting computed models to the distance calibrations, and these interpretations are robust.

RESULTS

Our probing experiments are based on the observation that Fe(II) can be tethered to particular locations on a molecule of interest (either protein or RNA), and can be used to generate hydroxyl radicals in a location-specific manner. The creation of hydroxyl radicals is initiated by the Fenton reaction. The hydroxyl radicals diffuse from the Fe(II) and quickly attack riboses in the RNA backbones, and cause strand scission within the phosphodiester backbone. These scissions can be detected with gel electrophoresis of the resulting fragments. The efficiency of strand scission at a particular location is related to the degree to which hydroxyl radicals diffuse to that location and react. Calibration experiments have shown that regions of the RNA backbone that are closer to the tethered Fe(II) are more frequently cut, and thus lead to more prominent bands on gel electrophoresis (Joseph et al., 1997).

Construction of defined complexes

Defined complexes were constructed by using ribosomes programmed with a 142-nt fragment of phage T4 gene 32 mRNA (Fig. 1). First, to probe the arrangement of P-site tRNA, we constructed complexes having

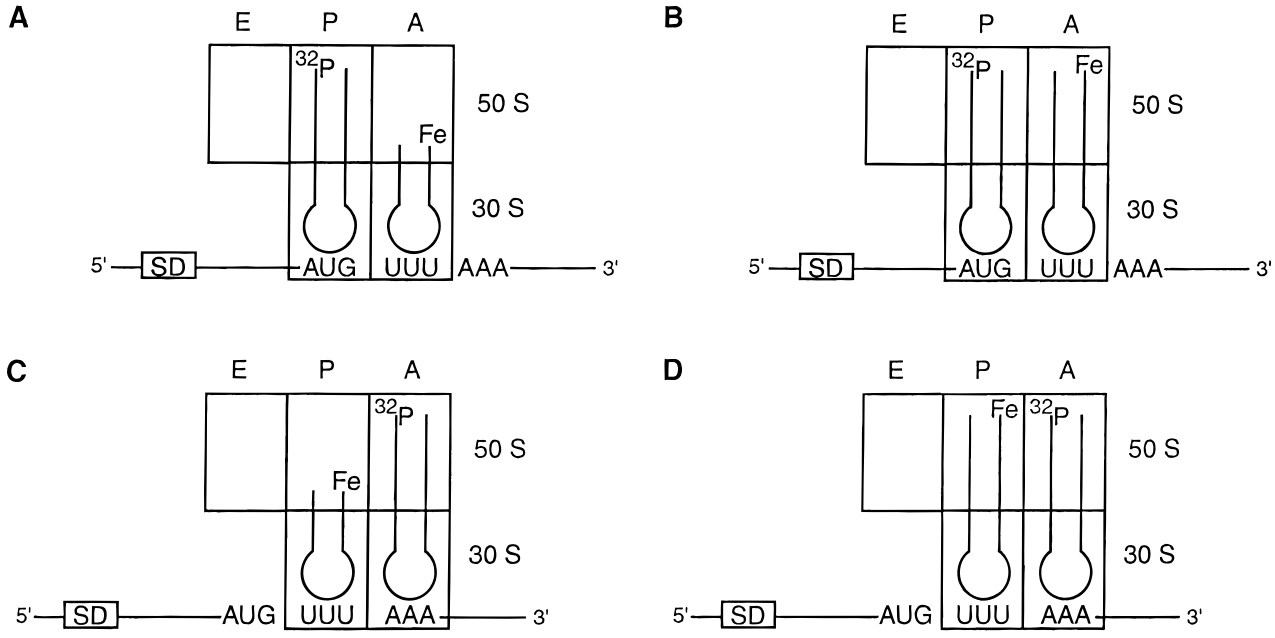

FIGURE 1. Strategy for probing the arrangement of tRNAs. **A**: Binding of deacylated $tRNA_f^{Met}[^{32}P]pCp$ to the AUG initiator codon in the P-site and 5′-Fe(II)-ASLs to the UUU codon in the A site using 70S ribosomes programmed with gene 32 mRNA. **B**: In the 5′-Fe(II)-$tRNA^{Phe}$ experiment, binding is identical to complex A except that 5′-Fe(II)-$tRNA^{Phe}$ binds in the A site. **C**: Binding of 5′-Fe(II)-ASLs to the UUU codon in the P site and deacylated $tRNA^{Lys}[^{32}P]pCp$ to the AAA codon in the A site using 70S ribosomes programmed with gene 32 mRNA. **D**: In the 5′-Fe(II)-$tRNA^{Phe}$ experiment, binding is identical to complex C except that 5′-Fe(II)-$tRNA^{Phe}$ binds in the P site. SD: Shine-Dalgarno sequence.

a deacylated $tRNA_f^{Met}[^{32}P]pCp$ in the ribosomal P site and either Fe(II)-ASLs4-33 or Fe(II)-$tRNA^{Phe}$ in the A site (Figs. 1A and B). Alternatively, to probe the arrangement of A-site tRNA, either Fe(II)-ASLs4-33 or Fe(II)-$tRNA^{Phe}$ was bound to the ribosomal P site and deacylated $tRNA^{Lys}[^{32}P]pCp$ to the A site (Figs. 1C and D). The ASLs are based on the yeast $tRNA^{Phe}$ sequence, so they bind specifically to ribosomes programmed with the codon UUU. ASLs and tRNAs with $[^{32}P]Cp$ ligated at the 3′ terminus do not bind to the ribosomal E site (Lill et al., 1988).

Fe(II)-ASL probing

We first probed $tRNA_f^{Met}[^{32}P]pCp$ bound to the ribosomal P site (P/P state) with a series of Fe(II)-ASLs4-33 bound to the small subunit ribosomal A site. A distinct pattern of cleavage in $tRNA_f^{Met}[^{32}P]pCp$ is observed that is dependent on ASL stem length (Fig. 2A) based on our quantification of the cleavage intensities. Hydroxyl radical-mediated strand scission was detected specifically at nucleotide residues 8–9, 25, 49–51, and 64–68 in $tRNA_f^{Met}[^{32}P]pCp$ (Fig. 3A). These four regions are located in the tRNA 5′ acceptor stem, D stem-loop, T stem-loop, and 3′ acceptor stem, respectively.

Next, we probed complexes with Fe(II)-ASLs4-33 bound to the ribosomal P site and $tRNA^{Lys}[^{32}P]pCp$ bound to the ribosomal A site. Again, we observe a distinct pattern of cleavage in $tRNA^{Lys}[^{32}P]pCp$ that is dependent on ASL stem length (Fig. 2B). Strand scission was detected at nucleotide residues 13–16, 21–24, and 39–41 in $tRNA^{Lys}[^{32}P]pCp$; the first two sets of

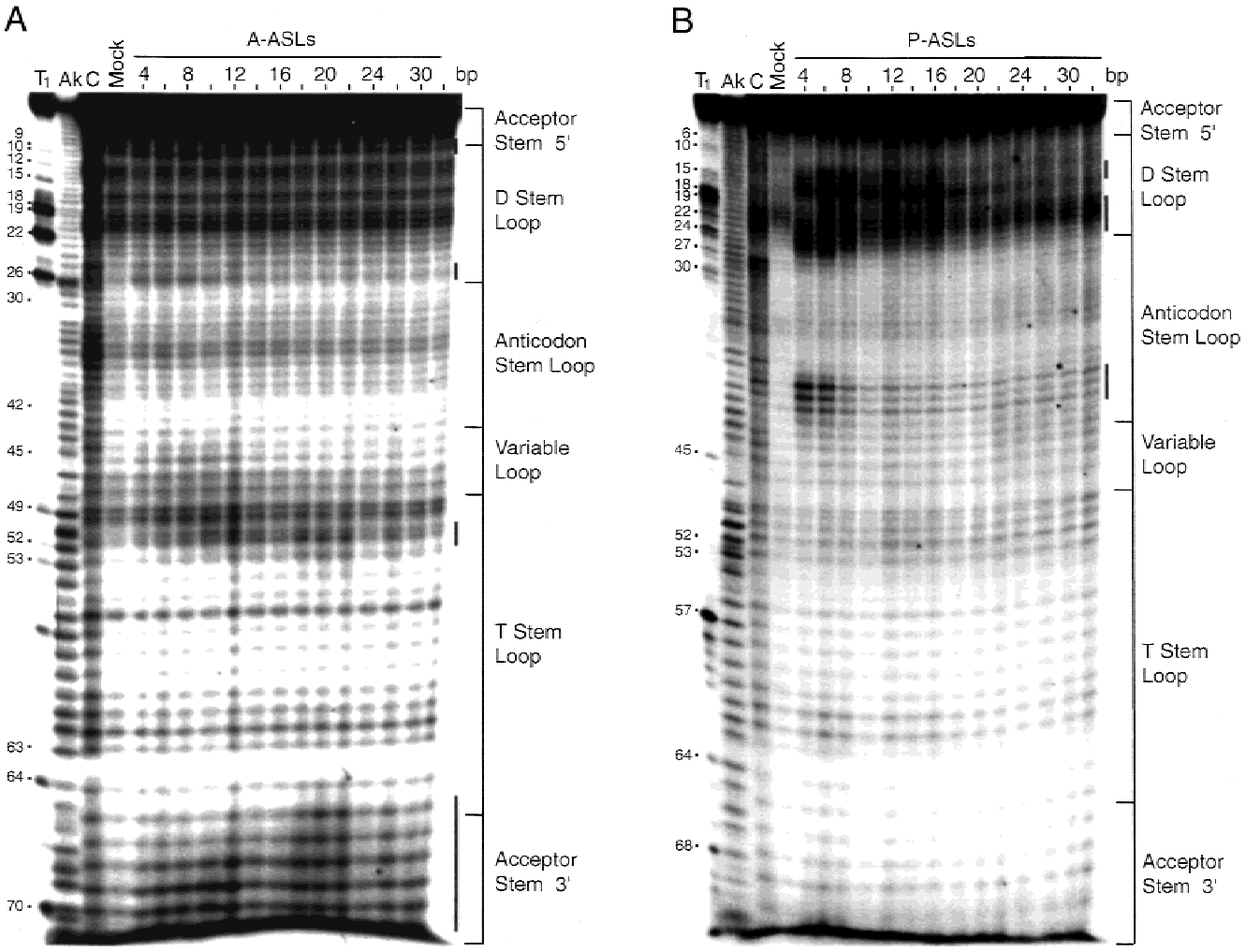

FIGURE 2. Strand scission of tRNAs by hydroxyl radicals generated from Fe(II)-ASLs. **A**: Strand scission of P site bound $tRNA_f^{Met}[^{32}P]pCp$ with Fe(II)-ASLs bound to the A site. **B**: Strand scission of A site bound $tRNA^{Lys}[^{32}P]pCp$ with Fe(II)-ASLs bound to the P site. T1: partial ribonuclease T1 digest of $tRNA[^{32}P]Cp$; Ak: alkaline hydrolysis of $tRNA[^{32}P]Cp$; C: reaction chemically treated as for the probing reaction, but containing an equimolar mixture of Fe(II)-ASLs 4–33 and no ribosome; Mock: reaction chemically treated as for the probing reaction, but in the absence of Fe(II)-ASLs 4–33. Lanes designated A-ASLs and P-ASLs are tRNA-ribosome complexes probed with Fe(II)-ASLs of increasing stem length, as indicated. Positions of strand scission are indicated by the bars.

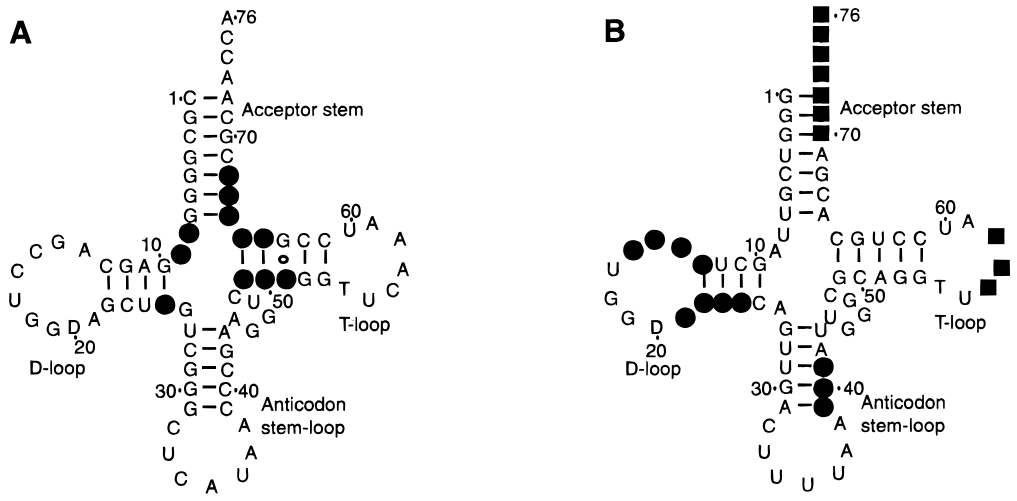

FIGURE 3. Sites of strand scission in (**A**) $tRNA_f^{Met}$ bound to the P site, and (**B**) $tRNA^{Lys}$ bound to the A site. Circles and squares represent strand scission of tRNAs by hydroxyl radicals generated from Fe(II)-ASLs and 5′-Fe(II)-$tRNA^{Phe}$, respectively. The numbering system is based on yeast $tRNA^{Phe}$.

cleavages are located in the D stem-loop, whereas the last set of cleavages is located in the anticodon stem-loop region of tRNA (Fig. 3B).

5′-Fe(II)-tRNA probing

Additionally, we probed the arrangement of A- and P-site tRNAs using Fe(II)-EDTA attached to the 5′ end of $tRNA^{Phe}$. We constructed complexes with $tRNA_f^{Met}$ [^{32}P]pCp bound to the P site and 5′-Fe(II)-$tRNA^{Phe}$ bound to the A site. No strand scissions were observed in P site-bound $tRNA_f^{Met}$[^{32}P]pCp (Fig. 4). Alternatively, we probed complexes with 5′-Fe(II)-$tRNA^{Phe}$ bound to the ribosomal P site and $tRNA^{Lys}$[^{32}P]pCp bound to the ribosomal A site. Strong cleavages were detected at positions 71–73, medium cleavages at position 70 (3′-acceptor stem) and weaker cleavages at positions 60–63 (T stem-loop) and 74–76 (3′-acceptor stem) (Fig. 3B). This result indicates that the 5′ end of P-site tRNA is close to the 3′-acceptor stem of A-site tRNA. Potential strand scission at positions 1–6 was obscured by the poor resolution of this part of the gel (Fig. 4).

Modeling the arrangement of A-site and P-site tRNAs in the ribosome

We used the dependence of cleavage intensity as a function of ASL stem-length, and the 5′-Fe(II)-tRNA probing data to compute the mutual arrangement of A-site and P-site tRNAs. Figure 5A shows the full atomic model built with 5′-Fe(II)-ASL and 5′-Fe(II)-tRNA probing data alone, and derived by fitting the $tRNA^{Phe}$ crystal structure (Bernstein et al., 1977) to the computed phosphate backbone model. The DGSOL program created the phosphate backbone model that best satisfied all experimental constraints and covalent chemical constraints. The resulting structure satisfies the experimental constraints with an average error of 1.07 standard deviation (SD) (maximum error of 2.25 SD). Although the FRET data were not used in constructing this model, the FRET constraints are satisfied with an average error of 0.78 SD (maximum SD of 1.83). The angle between these two tRNA molecules is 45°. The 3′CCA ends are 26.6 Å apart.

The best model built with 5′-Fe(II)-ASL and 5′-Fe(II)-tRNA probing data, but also incorporating constraints imposed by mRNA–tRNA codon–anticodon interactions was also produced by DGSOL (Fig. 5B) and was very similar to the model of Figure 5A [within 0.1 Å root mean square deviation (RMSD)]. Once again, although the FRET data were not used in constructing this model, it satisfied the FRET data as well as the model computed without constraining mRNA–tRNA interactions.

The PROTEAN program built the phosphate backbone of the structure best satisfying the pooled experimental data (all 5′-Fe(II)-ASL and 5′-Fe(II)-tRNA data, as well as previously published FRET data) along with constraints imposed by interactions with mRNA. The resulting structure satisfies all distance constraints with an average error of 1.20 SD (maximum 3.47 SD). The angle between the two tRNA molecules is 44°; their 3′CCA ends are 23.5 Å apart. Figure 5C shows the full atomic version of this structure. The mRNA in this model was built with MC-SYM II, as described in the Materials and Methods section. The anticodon loop bases are in their crystallographic conformation. The phosphate atoms of this structure have an RMSD of 3.39 Å to the structure built with 5′-Fe(II)-ASL and 5′-Fe(II)-tRNA probing data alone, and an RMSD of 0.1 Å to a struc-

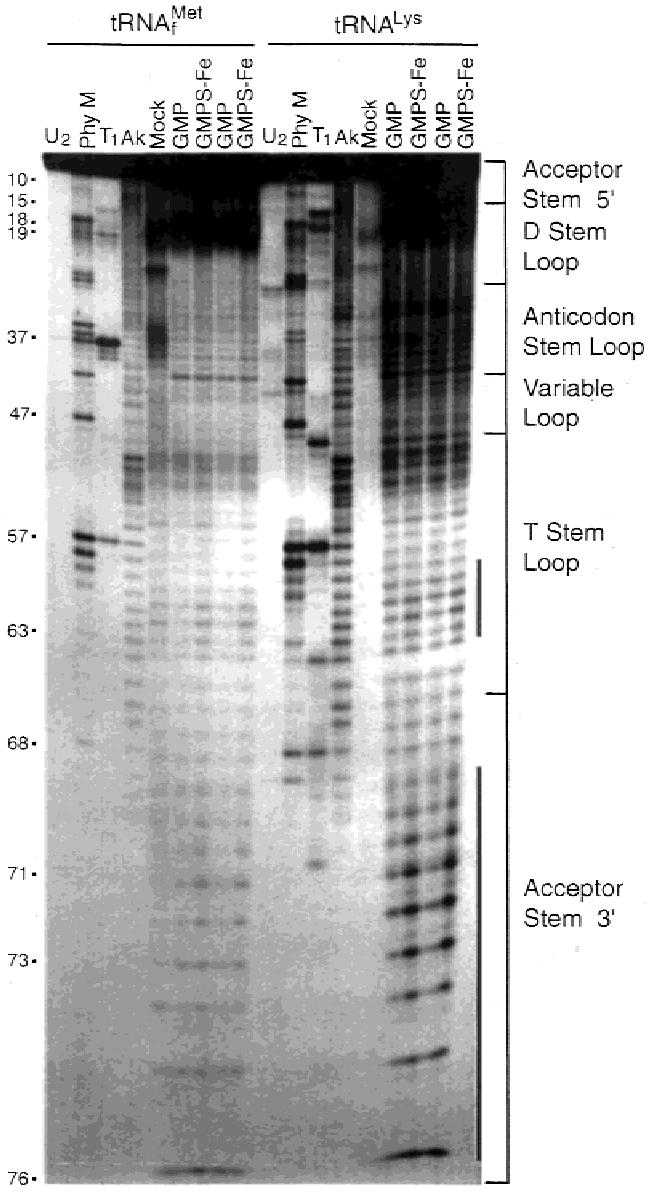

FIGURE 4. Strand scission of tRNAs by hydroxyl radicals generated from 5′-Fe(II)-tRNA. tRNA$_f^{Met}$, complexes with tRNA$_f^{Met}$[^{32}P]pCp bound to the P site, and either tRNA^{Phe} (GMP) or 5′-Fe(II)-tRNA^{Phe} (GMPS-Fe) bound to the A site. tRNA^{Lys}, complexes with tRNA^{Lys} [^{32}P]pCp bound to the A site, and either tRNA^{Phe} (GMP) or 5′-Fe(II)-tRNA^{Phe} (GMPS-Fe) bound to the P site. Lanes U2, Phy M, and T1 are enzymatic sequencing of tRNA[^{32}P]pCp using the respective ribonucleases; Ak: alkaline hydrolysis of tRNA[^{32}P]pCp; Mock: reaction chemically treated as for the probing reaction, but in the absence of ribosome. Positions of strand scission are indicated by the bars.

ture built with all data but no explicit mRNA (not shown). The details of codon–anticodon interaction are shown in Figure 6. The anticodons (positions 34–36) are stacked and interact with the corresponding codons (positions 1–2 and 4–5) through Watson–Crick base pairs and through G-U wobble pairs (positions 3 and 6). The mRNA backbone is kinked between the two codons to facilitate codon–anticodon interaction, mainly by accommodation of ϵ and ζ torsion angles (Table 1).

A CPK rendering of the full atomic model of the tRNAs showing the sites of strand scission is presented in Figure 7. Only one surface of each tRNA is attacked by hydroxyl radicals and this surface must face the other tRNA in the ribosome, unambiguously constraining the tRNAs in the S orientation. The 3′-CCA ends of the two tRNAs are 23.5 Å together in our model (Fig. 7C). The sites of strand scission in A-site tRNA from Fe(II) tethered to the 5′-end of P-site tRNA map to the T stem and acceptor stem of (Fig. 7, yellow).

We also built numerous models based only on the FRET data and distance constraints on the 3′CCA ends of the tRNAs and on the anticodon regions of the tRNAs (data not shown). The models satisfied the FRET constraints with an average error of around 0.6 SD (about 1.0 SD maximum). Importantly, these models did not satisfy the ASL and 5′P data very well, with (for the best result) an average error of over 2.0 SD and a maximum error of over 5.9 SD for those data points. The angle between these two tRNA molecules ranged from 18° to 75° and the 3′CCA ends distances ranged from 22.49 to 23.42 Å.

Figure 8 shows the actual distances in the full atomic model for the ASL and 5′P constraints that were assigned cleavage strengths of strong, medium, and weak. For each category, the points denote the actual distance of each experimental constraint in the model. The largest deviation from the previously estimated maximum target distances (Noller et al., 1990) was approximately 5 Å for some strong constraints. Here, strength of hydroxyl-radical cleavage determines the *maximum* distance between probe and target, because, for example, a weak cleavage could result for a close distance in which the target is obstructed, or where the reactive face of the ribose faces away from the probe (Balasubramanian et al., 1998).

DISCUSSION

Establishing the mutual orientation of the A-site and P-site tRNAs on the ribosome has been a topic of spirited discussion for more than 30 years. Even before the X-ray crystal structure of tRNA was solved, models were proposed for the arrangement of tRNAs on the ribosome. Fuller and Hodgson (1967) modeled codon–anticodon interaction and proposed that nt 34–38 in the anticodon loop of tRNA are 3′-stacked in the standard A-RNA conformation. Additionally, the mRNA in their model was kinked between the two codons to allow simultaneous recognition of adjacent codons by two tRNA anticodons. After the X-ray structure of tRNA was solved, Rich (1974) proposed a model in which the T loop of A-site tRNA faces the D loop of P-site tRNA at an angle of 90° between the tRNA planes. An alternate arrangement was proposed by Sundaralingam et al. (1975) in which the D loop of A-site tRNA faces the T loop of P-site tRNA, with a 60° angle between the planes

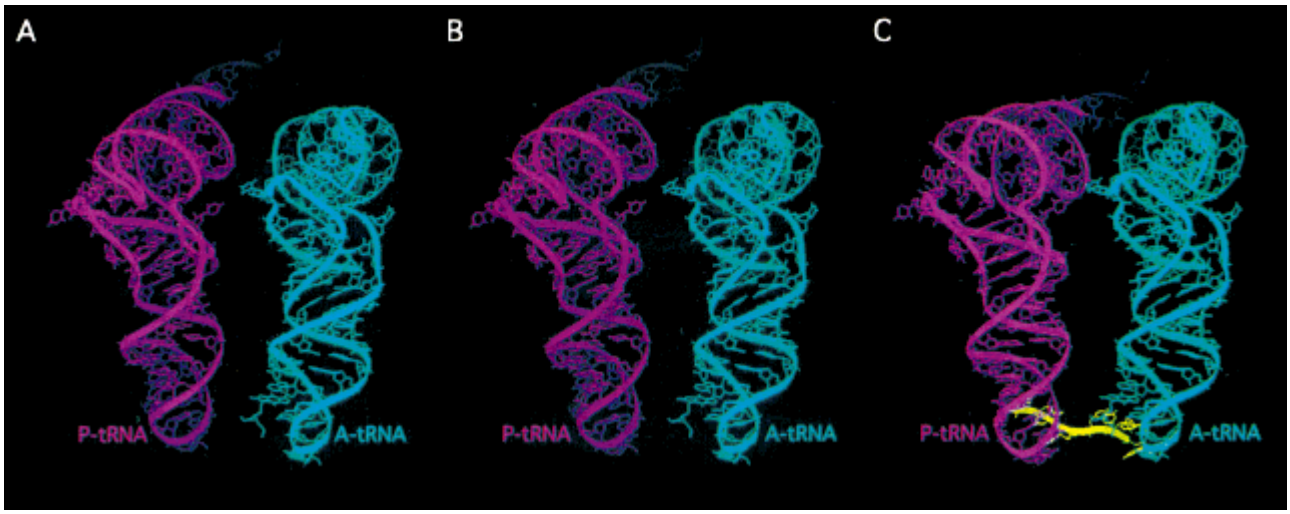

FIGURE 5. Models for the arrangement of tRNAs. Models for the arrangement of A-site and P-site tRNAs based on (**A**) 5′-Fe(II)-ASL and 5′-Fe(II)-tRNA probing data only, (**B**) 5′-Fe(II)-ASL, 5′-Fe(II)-tRNA probing data and mRNA constraints, and (**C**) 5′-Fe(II)-ASL, 5′-Fe(II)-tRNA probing data, mRNA constraints, and FRET data. The tRNA pairs are shown with the P-site tRNA (magenta) on the left, the A-site tRNA (cyan) on the right, and the mRNA (yellow) at the bottom. The anticodon stem-loops of the tRNAs are at the bottom and their acceptor ends are at the top facing away from the reader. The orientation of A-site tRNA is similar in **A**, **B**, and **C**.

of the two tRNAs. These two mutually exclusive arrangements have been designated as the R and S orientations, respectively (Lim et al., 1992).

Fluorescence resonance energy transfer experiments provided important constraints for modeling the mutual arrangement of tRNAs (Fairclough & Cantor, 1979b; Wells & Cantor, 1980; Johnson et al., 1982; Paulsen et al., 1983). Paulsen et al. (1983) proposed a model with a $60 \pm 30^\circ$ angle between the A- and P-site tRNAs, but were unable to distinguish between the R and S orientations using FRET constraints. Although the FRET data by themselves were insufficient to decide this issue, they served the useful purpose of eliminating models that were inconsistent with the measured distances.

Based on a stereochemical analysis of the peptidyl transferase reaction, Spirin and Lim (1986) proposed

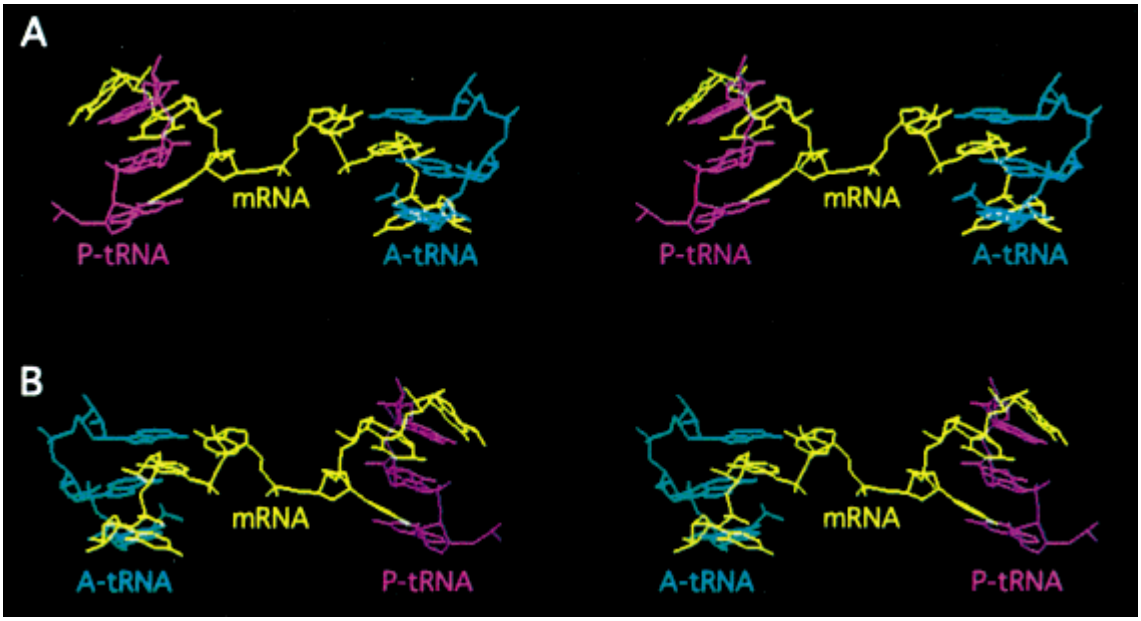

FIGURE 6. Stereo pairs showing codon–anticodon interaction in model C. **A**: The tRNA anticodon nucleotides are in front and the mRNA is behind. **B**: 180° rotation of **A**. The color coding is the same as in Figure 5.

TABLE 1. Torsion angles of mRNA nucleotides in model C.

mRNA residue number	Torsion angles					
	α	β	γ	δ	ϵ	ζ
1	None	178.96	27.10	95.47	−177.2	−87.38
2	−50.14	−165.9	67.17	73.50	−147.8	−67.21
3	−44.84	161.10	74.24	96.32	−68.56	78.85
4	−65.82	179.49	58.78	78.26	−141.3	−79.45
5	−63.37	179.90	54.19	86.99	−109.9	−100.0
6	−62.28	146.28	67.94	99.55	None	None

an R orientation with a 100° angle between the two tRNAs. Ofengand et al. (1986), based on tRNA crosslinks to 30S subunit protein S19 and other biochemical data, proposed a model with the tRNAs in the S orientation with an angle of 65° between the tRNA planes. A detailed stereochemical model using the crystal structure of tRNA and incorporating the FRET data was proposed by McDonald and Rein (1987), who maintained the tRNA crystal structures as rigid bodies and manipulated the conformation of the mRNA. Their model has an S orientation with an approximately 45° angle between the tRNA planes and a 33° kink between the two mRNA codons. Models with mRNA fixed in an idealized A-form geometry, deforming the anticodon loops of the tRNAs from the crystal structure (Prabahakaran & Harvey, 1989), or where both the mRNA codons and tRNA anticodon loops have altered conformations (Easterwood et al., 1994) were also proposed; the tRNAs in these models are in the S orientation with an angle of approximately 45°. While the S orientation is preferred in some of the models based on crosslinking and chemical protection studies (Stern et al., 1988; Wower et al., 1989, 1993; Noller et al., 1990; Nagano et al., 1991; Nagano & Nagano, 1997), Lim and coworkers invoked extensive tRNA, mRNA, and rRNA crosslinking data to derive a model with R orientation (Lim et al., 1992; Spirin et al., 1993). Based on more recent data, Brimacombe and coworkers favor the S orientation with a 50° angle between the tRNA planes (Brimacombe, 1995; Mueller et al., 1997). Interestingly, results from in vivo genetic analysis provide evidence that the 5′ side of the P-site anticodon stem-loop is in proximity to the 3′ side of the A-site anticodon stem-loop (Smith & Yarus, 1989), leading these authors to model the tRNAs in the S orientation (not the R orientation as reported in their paper) with an angle of 50°.

Cryoelectron microscopy and three-dimensional image reconstruction of vacant ribosomes was used as an envelope to constrain the arrangement of tRNAs in the R orientation with a 60° angle between the A- and P-site tRNAs (Stark et al., 1997a). Recently, cryoelectron microscopy was used to directly visualize the arrangement of tRNAs in the ribosome. In one study (Malhotra et al., 1998), three tRNAs bound to poly (U)-programmed 70S ribosomes were visualized at 25 Å resolution. The angle between the A-site and P-site tRNAs was 160° and the orientation of the tRNAs was intermediate between the R and S orientations. In contrast, another cryoelectron microscopy study (Spirin, 1983) compared pre- and posttranslocational states of the ribosome and found the angle between the tRNAs to be 50° and in the S orientation. Nierhaus et al. (1998) used a proton-spin contrast variation technique to compare the pre- and posttranslocational states and concluded that the angle between the A- and P-site tRNAs is 110 ± 10°. They were unable to distinguish between the R and S orientations. Most recently, the crystal

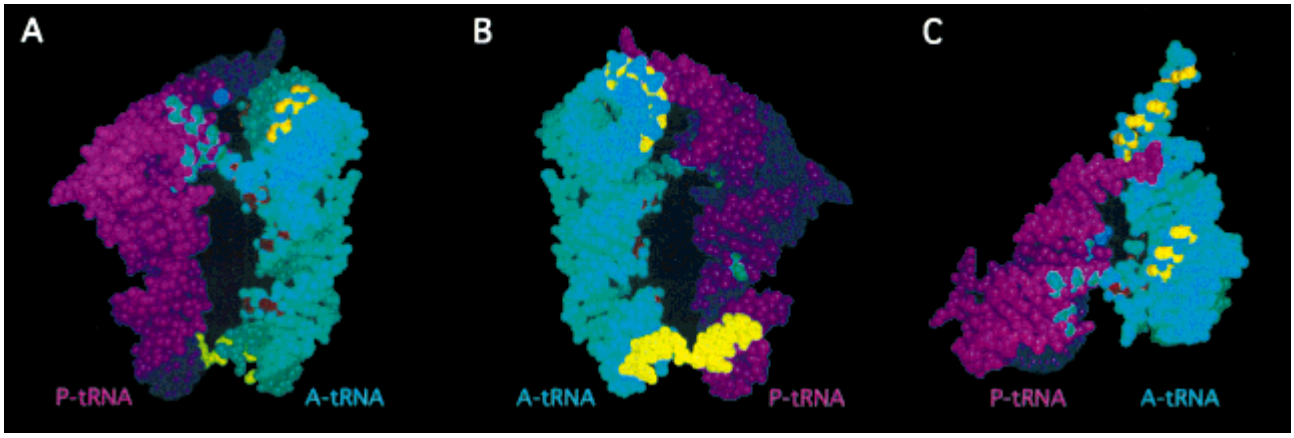

FIGURE 7. Sites of hydroxyl radical-mediated strand scissions mapped on model C. **A**: CPK rendering of model C showing P tRNA (magenta) on the left, A tRNA (cyan) on the right, and mRNA at the bottom (yellow). The sites of strand scissions from Fe(II) tethered to 5′ ends of ASLs are indicated on P and A tRNAs in green and red, respectively. The sites of strand scissions from Fe(II) tethered to 5′ end of P tRNA are indicated in gold on A tRNA. The 3′-CCA ends are pointing away from the reader in this view. **B**: 180° rotation of **A**. **C**: A view from the top with the model oriented as in **A**. Only one surface of the tRNA pair is cleaved by hydroxyl radicals indicating that these sides face each other in the ribosome.

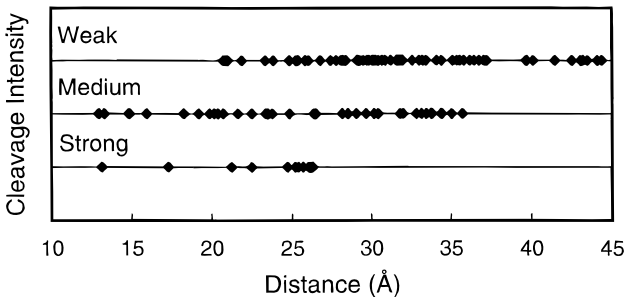

FIGURE 8. A plot of strength of hydroxyl radical strand scission versus actual distance between the probing position and sites of strand scission in model A. For each strength category (strong, medium, weak), the points denote the actual distance within the computed model A corresponding to the experimental constraint.

structure of the 70S ribosome (Cate et al., 1999) seems to show the A- and P-site tRNAs to be almost parallel to each other in the S configuration.

Our results show that the 5′-Fe(II)-ASL and 5′-Fe(II)-tRNA probing data alone are sufficient to build a reliable model for the arrangement of the tRNAs in the ribosome (Fig. 5A). In fact, even though the FRET data were not used as constraints for this model, they are nevertheless well satisfied by it (Table 2). Incorporation of the FRET data results in very little change in the structure. However, we were unable to build a structure using the FRET data alone that satisfied the 5′-Fe(II)-ASL and 5′-Fe(II)-tRNA probing data, indicating that the latter have a higher information content.

It is important to note that in our first computation (Fig. 5A), the anticodons are brought together in space, as are the 3′-CCA ends without any explicit constraints on either position—only the probing data were used in these computations. The terminal 3′ phosphates are 23.5 Å apart, when we model the 3′ terminal phosphate chain (bases 73–76) as they appear in the tRNA crystal structures. It is likely that for the two 3′ ends to bring together the growing polypeptide and the next amino acid, in preparation for the peptide bond formation step, the detailed structures of these two termini have to change. The conformational freedom of the RNA chains from bases 73 to 76 is substantial, and capable of bringing the two amino acids into the correct approximation within the context of our modeled relative tRNA locations. The introduction of constraints to ensure interaction of both anticodons with a single mRNA molecule and to ensure that the 3′-CCA ends are close to one another does not significantly change the relative positions of the two tRNA molecules. These observations provide strong evidence that the probing constraints provide abundant and biologically relevant information.

TABLE 2. Comparison of our models with FRET distance measurements (Johnson et al., 1982; Paulsen et al., 1983).

A-site tRNA residue	P-site tRNA residue	Distances in Angstroms			
		FRET	Model A	Model B	Model C
37	37	24 ± 4	23.99	24.06	23.32
37	16, 17	46 ± 12	54.96	54.94	54.13
16, 17	37	38 ± 10	39.83	39.86	39.66
16	16, 17	35 ± 9	34.17	34.17	33.47
8	8	26 ± 4	29.66	29.66	30.36

Our models appear to be in agreement visually with the cryoelectron microscopy model of van Heel and coworkers (Stark et al., 1997a) although their data are completely independent of the approach used here. Also, our model A has an RMSD to the A- and P-site tRNAs in the 70S crystal structure (Cate et al., 1999) of 5.8 Å. The angles between the A- and P-site tRNAs in our models fall consistently between 43 and 53° (Fig. 5). Our models are most compatible with the model proposed by Easterwood and coworkers (1994), which is in the S configuration. Models in the R configuration do not satisfy the constraints as well as those in the S. Table 3 summarizes the average and maximum constraint errors for two of our models (A and C), the Easterwood model, and the Lim/Mueller model (Lim et al., 1992; Mueller et al., 1997), as well as the RMSD of all these models from our model A. Our full atomic model of the crystal structure of A-site and P-site tRNA docked to mRNA is one possible structure compatible with these data (Fig. 5C). This structure was built with the crystallographically determined positions of the anticodon loops, and without modifying the tRNA structures at all. No energy minimization was used. We were able to build mRNA models in other cases by allowing small deviations in the tRNA structures, with RMS deviations from the crystal structure ranging from 1 to 3 Å (Fig. 5B). In these models, the anticodon side chains remained stacked, but deviated from their crystallographic positions. It is likely that the anticodon bases actually do move slightly upon binding mRNA, and so the model we show in Figure 5C may be somewhat overconstrained. It thus represents a proof of concept for these tRNA orientations. Some of the intermolecular contacts in the tRNA crystal structures also suggest ways in which the codon-to-anticodon interactions can affect the conformation of the anticodon loop. For example, the anticodon–anticodon interaction between tRNA molecules within the crystallographic asymmetric unit in the crystal structure of $tRNA^{Asp}$ shows one way in which codon–anticodon pairing might be accommodated while retaining the 3′ stacking geometry of the anticodon loop (Westhof et al., 1988).

In our model building, we have classified the distances implied by our experiments into the three categories of strong, medium, and weak. Figure 8 shows that the structures we have built are not very sensitive

TABLE 3. Comparison of our models with Easterwood et al. (1994) and Lim/Mueller (1992, 1997) models.

	Constraints						
	5′-Fe(II)-tRNA data		5′-Fe(II)-ASL data		FRET data		RMSD to
Models	Avg. SD	Max. SD	Avg. SD	Max. SD	Avg. SD	Max. SD	Model A
Model A	1.50	2.03	1.02	2.25	0.78	1.83	0.00
Model C	1.97	3.21	1.13	3.47	0.91	2.18	3.18
Easterwood et al.	1.20	3.21	1.68	5.24	1.17	2.54	8.61
Mueller/Lim et al.	1.73	3.24	2.73	3.66	1.61	4.13	24.25

to this classification. For example, the medium range encloses most of the weak and strong range, so assigning a constraint as medium instead of weak or medium instead of strong does not lead to unsatisfied distance constraints. Only the case of overestimating the strength of cleavage would lead to a possible conflict in the satisfaction of a distance constraint. The substantial overlap of the distance ranges associated with each intensity category is, of course, expected, because hydroxyl-radical attack of a nearby target can be attenuated by an intervening object; however, we expect the upper boundaries to be sharper (e.g., a strong cleavage cannot occur at a remote target).

The FRET data, when used alone, posed problems for both of the algorithms we used. Both programs produced numerous diverse solutions that seemed to be the result of local minima problems. The errors of these structures were higher than the best resulting models, but the frequency with which these higher error solutions were generated was much greater than for those which satisfied the FRET data well. It could be that this data set is more problematic because it consists of multiple distances between only six points, and is therefore highly degenerate.

In our models, we assume that tRNAs maintain their crystallographically determined conformation when bound to the ribosome. It is possible that tRNAs undergo significant conformational change when bound to the ribosome as suggested by the crystal structures of tRNA–synthetase complexes (Rould et al., 1989; Ruff et al., 1991) and by low-resolution cryoelectron microscopy difference maps of tRNA–ribosome complexes (Malhotra et al., 1998).

To understand the molecular mechanism of translation, it is essential to elucidate the mutual arrangement of tRNAs on the ribosome. So far, at least a half-dozen different binding states of tRNA have been described (Green & Noller, 1997). In these studies, the tRNAs are bound in the A/A and P/P states, corresponding to the classical A and P sites. They are in the S orientation with the P tRNA on the left and A tRNA on the right as viewed from the 30S toward the 50S subunit (Fig. 7A). The anticodon stem-loops are at the bottom, interacting mainly with the 30S subunit and mRNA; the 3′-CCA ends are at the top, interacting with the 50S subunit. Although the 3′ termini of the two tRNAs are insufficiently close to allow peptide bond formation, flexibility of their single-stranded 3′-ACCA termini could allow a closer approach. Placement of A-site tRNA on the right is consistent with the interaction of the EF-Tu ternary complex near the L7/L12 stalk at the right of the 50S subunit (Girshovich et al., 1986; Stark et al., 1997b). Also, in the crystal structure of the EF-Tu:GDPNP:tRNA ternary complex, the T-loop side of the A-site tRNA is in contact with EF-Tu (Nissen et al., 1995). Therefore, this side cannot face P tRNA, consistent with the S orientation.

An important ribosomal function is translocation, the coordinated movement of the tRNA–mRNA complex within the ribosome following peptide bond formation (Kaziro, 1978; Spirin, 1985; Czworkowski & Moore, 1996; Wilson & Noller, 1998). During translocation, tRNAs move from right to left from A site to P site as shown in Figure 7A. Our model predicts that translocation of A-site tRNA into the P site could be accomplished by a rotational movement of about 45° around an axis drawn from the 3′-CCA end through the anticodon stem-loop of the A-site tRNA, coupled with a translational movement of about 24.5 Å from right to left.

Interestingly, we do not detect any cleavages in the anticodon stem-loop region of P tRNA, consistent with the previous observation that the anticodon stem-loop of P tRNA is protected from hydroxyl radicals by the 30S subunit (Hüttenhofer & Noller, 1994), most likely by features of 16S rRNA that line the cleft of the 30S subunit. Nor do we detect any cleavages in the 3′-CCA end of P tRNA from Fe(II) tethered to the 5′ terminus of A tRNA. The 3′ end of P tRNA may be shielded from hydroxyl radicals by its interactions with the 2250 loop (Samaha et al., 1995) and other features of 23S rRNA.

These studies have focused on two particular sets of tRNA binding complexes. There are currently believed to be as many as eight (or possibly more) identifiable binding states for tRNA (Wilson & Noller, 1998), of which our complexes likely represent a single state. The geometry of tRNA within the ribosome is likely to deviate dramatically from the one presented here in some of these other states.

MATERIALS AND METHODS

In vitro transcription of gene 32 mRNA and ASLs

Gene 32 mRNA fragment was transcribed in vitro from a PCR-generated DNA template using T7 RNA polymerase and gel purified, all as described (Hüttenhofer & Noller, 1992). Anticodon stem-loop analogs of tRNA were also transcribed in vitro using T7 RNA polymerase. During transcription, a phosphorothioate was introduced at the 5′ end of the ASLs by transcribing in the presence of a fivefold molar excess of 5′-guanosine–phosphorothioate over each NTP, essentially as described (Joseph et al., 1997; Joseph & Noller, 1996). The 5′-GMPS-ASLs were derivatized with Fe(II)BABE (DeRiemer et al., 1981; Rana & Meares, 1990) and purified (Joseph et al., 1997). Similarly, $tRNA^{Phe}$ was transcribed from plasmid p67CF10 (Sampson et al., 1989) and derivatized with Fe(II)BABE as described (Joseph & Noller, 1996). Deacylated, native *Escherichia coli* $tRNA^{Met}$ and $tRNA^{Lys}$ were labeled at their 3′ termini by ligating [^{32}P]pCp using T4 RNA ligase (England et al., 1980) and gel purified as described (Hüttenhofer & Noller, 1992).

Binding of tRNA and ASLs to 70S ribosomes

For probing the arrangement of P-site tRNA, complexes containing deacylated $tRNA_f^{Met}$[^{32}P]Cp bound to the ribosomal P site and either Fe(II)BABE-ASLs or Fe(II)BABE-$tRNA^{Phe}$ bound to the A site were formed by using ribosomes programmed with gene 32 mRNA. Briefly, 10 pmol (1.0 μM) tight couple 70S ribosomes were activated by incubating for 10 min at 42 °C and 10 min at 37 °C in binding buffer (80 mM K-cacodylate, pH 7.2, 20 mM $Mg(OAc)_2$, 150 mM NH_4Cl) followed by addition of 30 pmol (3.0 μM) gene 32 mRNA and incubating for 6 min at 37 °C. Next, 10^5 cpm $\approx$ 1 pmol (0.1 μM) *E. coli* $tRNA_f^{Met}$[^{32}P]pCp were added and the complex was incubated for 30 min at 37 °C, followed by addition of 10 pmol (1.0 μM) unlabeled *E. coli* $tRNA_f^{Met}$ and incubating for 15 min at 37 °C to fill the remaining ribosomal P sites. The A site was next filled by adding 10 pmol (1.0 μM) Fe(II)BABE-ASLs or Fe(II)BABE-$tRNA^{Phe}$ to the above complex and incubating for 30 min at 37 °C, followed by 30 min on ice.

For probing the arrangement of A-site tRNA, complexes containing either Fe(II)BABE-ASLs or Fe(II)BABE-$tRNA^{Phe}$ bound to the P site and deacylated $tRNA^{Lys}$[^{32}P]pCp bound to the A site were formed by using ribosomes programmed with gene 32 mRNA as described above. Briefly, 10 pmol (1.0 μM) tight couple 70S ribosomes were activated by incubating for 10 min at 42 °C and 10 min at 37 °C in binding buffer, followed by addition of 30 pmol (3.0 μM) gene 32 mRNA and incubating for 6 min at 37 °C. Next, 10 pmol (1.0 μM) of either Fe(II)BABE-ASLs or Fe(II)BABE-$tRNA^{Phe}$ were added and the complexes were incubated for 30 min at 37 °C to fill the P site; this was followed by addition of 10^5 cpm $\approx$ 1 pmol (0.1 μM) *E. coli* $tRNA^{Lys}$[^{32}P]pCp and further incubation at 37 °C for 30 min. Finally, the remaining unfilled A sites were filled by adding 10 pmol (1.0 μM) of *E. coli* $tRNA^{Lys}$ and incubating for 5 min at 37 °C followed by 30 min on ice. Binding was performed in buffer containing 20 mM Mg^{2+} to favor efficient ASL binding to the ribosome. Additionally, at 20 Mg^{2+}, deacylated tRNAs bind to the ribosome in the classical A/A and P/P states (Moazed & Noller, 1989).

Directed hydroxyl radical probing

Directed hydroxyl radical probing using Fe(II)BABE-derivatized ASLs or $tRNA^{Phe}$ was performed essentially as described (Joseph & Noller, 1996; Joseph et al., 1997). Briefly, hydroxyl radical strand scission was initiated by the addition of ascorbate (5 mM final concentration) and hydrogen peroxide (0.05% final concentration) to 10 μL of the reaction mixture (see above) followed by incubation for 10 min at room temperature. Reactions were stopped by addition of 300 μL of cold ethanol and 3 M Na acetate (0.3 M final concentration) and quick freezing in a dry ice–ethanol bath. Samples were extracted three times with phenol and three times with chloroform to remove ribosomal proteins, and the tRNA [^{32}P]pCp recovered by ethanol precipitation and resuspended in 10 μL of loading buffer (95% formamide, 20 mM EDTA, 0.05% xylene cyanol, 0.05% bromophenol blue). Alkaline hydrolysis and enzymatic sequencing of $tRNA_f^{Met}$[^{32}P]pCp and $tRNA^{Lys}$[^{32}P]pCp were performed using ribonucleases T1 (G specific), Phy M (A, U specific), and U2 (A, G specific) as per the manufacturer's (Pharmacia) recommended protocol. Reactions were analyzed on 10% denaturing polyacrylamide gels and were quantified using a Molecular Dynamics PhosphorImager. Gels were scanned and ImageQuant software was used to measure counts within a rectangle (volume integration) enclosing a band corresponding to a site of strand scission in the tRNA. Additionally, bands located at similar positions on the gel in the mock reaction were quantified and used for comparing cleavage intensity at different positions in the gel. The values were manually classified as "strong" if the counts were $\geq$2.5$\times$ mock value, "medium" if the counts were $<$2.5$\times$ but $>$1.5$\times$ mock value, and "weak" if the counts were $<$1.5$\times$ but $>$1.25$\times$ mock value. These strength categories were then translated into distance constraints to use the experimental data with numerical model building programs. Strong interactions were assigned a range of 0–22 Å, medium interactions were given a range of 12–36 Å, and weak interactions were given a range of 20–44 Å. These distances were based on calibration experiments described (Joseph et al., 1997).

Modeling the arrangement of tRNAs

For model building, the crystal structure of $tRNA^{Phe}$ (Kim et al., 1973) (including the positions of the base side chains in the anticodon loop) was used as a rigid body. In addition, models of the interaction between the P-site and A-site tRNA were built on the assumption that the interactions with mRNA occur at the same time. Models were built with two distance-based algorithms: PROTEAN (Altman, 1995) and DGSOL (More & Wu, 1997) to maximize the probability of sampling all important conformations. PROTEAN is a probabilistic least-squares algorithm (Chen et al., 1998) that computes distance constraints with a mean value and a variance (uncertainty). The starting backbone structure used by PROTEAN was generated by a random walk, with each step equal to the average distance between consecutive phosphates in an RNA molecule. DGSOL is a distance geometry program (More & Wu, 1997), that uses distance ranges (minimum and maximum)

as input data. DGSOL also starts with random atomic coordinates as part of its computation.

Three types of distance data were supplied to these programs, in different combinations as detailed below. First, the data from directed hydroxyl probing were used, with distance ranges between associated phosphates for strong, medium, and weak categories of 0–22, 12–36, and 20–44 Å, respectively. For PROTEAN, the means of these ranges were taken, with a variance (designed to have the ranges fall within ±2 SD) of (maximum − minimum)^2/16. In addition, the mean distance for the strong category was increased from 11 to 15 Å to minimize van der Waals overlap violations. Second, the distance constraints derived from published FRET data were used (Johnson et al., 1982; Paulsen et al., 1983). Finally, the crystal structure of yeast tRNA^{Phe} was used to create a list of distances between phosphate atoms in the tRNA structure, to ensure that the crystal structure of each tRNA was reproduced in the calculations. The variance for these crystallographic distances was taken to be 0.01 Å^2.

Four structural computations were performed using the modeling programs and different combinations of constraints:

1. Hydroxyl probing data only. Phosphate backbone structures of the interacting A-site and P-site tRNAs were built with the 5′Fe(II)-ASL and 5′-Fe(II)-tRNA probing data as input. No other information was provided to the program about the relative positions of the two tRNA molecules.
2. Hydroxyl probing data with mRNA. Phosphate backbone structures were built with the 5′Fe(II)-ASL and 5′-Fe(II)-tRNA probing data, but now including a reduced-atom representation of the six mRNA bases constrained with distances to the anticodon loops of the tRNAs. The mRNA bases (and the three associated anticodon loop bases) were represented by a phosphate atom and two atoms from the base side chain (O4 and N3 for mRNA uracils Watson–Crick base paired to adenine, O2 and N3 for mRNA uracil bases wobble base paired to guanine; N6 and N1 for tRNA adenine, N1 and N3 for tRNA guanine). Distance constraints compatible with Watson–Crick and Wobble base pairing were used to constrain the relative locations of mRNA and anticodon loops.
3. Hydroxyl probing and FRET data with mRNA. Phosphate backbone structures were built using 5′Fe(II)-ASL and 5′-Fe(II)-tRNA probing data, as well as the published FRET data. Constraints to the reduced-atom mRNA representation were used as described in 2.
4. FRET data and inferred distances. Finally, phosphate backbone structures were built using the FRET data alone, along with distance constraints between the 3′-ACCA final phosphates (21 ± 4 Å), as well as constraints between base 35 of the respective anticodons (28 ± 4 Å) added.

For all models created, the chiralities of the resulting tRNA structures were checked and models with incorrect handedness were discarded. Model errors were calculated as: ((actual distance in model − target mean distance)/constraint standard deviation). This error represents a residual normalized by the estimated precision of individual measurements. Full-atomic models were created by fitting the phosphate backbones to the tRNA crystal structures. tRNA angle measurements were computed between the two planes defined by bases 23, 61, and 72 within the two tRNA molecules.

MC-SYM II was used for modeling the detailed conformation of mRNA (Major et al., 1991). A six-base mRNA strand with sequence UUUUUU was created. Anticodon loop positions for A-site and P-site tRNA were fixed at the positions determined by fitting the crystal structure to the computed phosphate backbone. An MC-SYM II script constrained each base in the mRNA to adopt a backbone conformation compatible with known allowed RNA torsion angles. The script also constrained the interaction of the mRNA with the two anticodon loops: Watson–Crick base pairing interactions were specified for codon positions one and two, and wobble base interactions were specified for the third codon position. The resulting full atomic mRNA model satisfied all these constraints.

ACKNOWLEDGMENTS

We thank J. Moran, D.P. Greiner, and C.F. Meares for helping with synthesis of BABE and members of the Noller lab for discussions. This investigation was supported (in part) by a California Division—American Cancer Society Fellowship, #1-38-97B, to S.J., by grant GM-17129 from the National Institutes of Health (NIH) to H.F.N., and by a grant to the Center for Molecular Biology of RNA from the Lucille P. Markey Charitable Trust. R.B.A. is supported by NIH LM-05652, LM-06422, National Science Foundation DBI-9600637 and grants from IBM and Sun Microsystems. M.L.W. is supported by a predoctoral fellowship from NIH GM-08294.

Received September 24, 1999; returned for revision October 29, 1999; revised manuscript received November 12, 1999

REFERENCES

Agrawal RK, Penczek P, Grassucci RA, Li Y, Leith A, Nierhaus KH, Frank, J. 1996. Direct visualization of A-, P-, and E-site transfer RNAs in the *Escherichia coli* ribosome. *Science 271*:1000–1002.

Altman RB. 1995. A probabilistic approach to determining biological structure: Integrating uncertain data sources. *Int J Human-Computer Stud 42*:593–616.

Balasubramanian B, Pogozelski WK, Tullius TD. 1998. DNA strand breaking by the hydroxyl radical is governed by the accessible surface areas of the hydrogen atoms of the DNA backbone. *Proc Natl Acad Sci USA 95*:9738–9743.

Bernstein FC, Koetzle TF, Williams, GJB, Meyer EF Jr, Brice MD, Rodgers JR, Kennard O, Shimanouchi T, Tasumi, M. 1977. The Protein Data Bank: A computer-based archival file for macromolecular structures. *J Mol Biol 25*:535–542.

Brimacombe R. 1995. The structure of ribosomal RNA: A three-dimensional jigsaw puzzle. *Eur J Biochem 230*:365–383.

Brimacombe R, Doring T, Greuer B, Junke N, Mitchell P, Mueller F, Osswald M, Rinke-Appel J, Stade K. 1993. Mapping the functional center of the Escherichia coli ribosome. In: Nierhaus KH, Franceschi F, Subramanian AR, Erdmann VA, Wittmann-Liebold B, eds. *The translational apparatus: Structure, function, regulation, evolution*. New York: Plenum Press.

Cate JH, Yusupov MM, Yusuopova GZ, Earnest TN, Noller HF. 1999. X-ray crystal structures of 70S ribosome functional complexes. *Science 285*:2095–2104.

Chen CC, Singh JP, Altman RB. 1998. The hierarchical organization of molecular structure computations. *J Computational Biol 5*:409–422.

Czworkowski J, Moore PB. 1996. The elongation phase of protein synthesis. *Prog Nucleic Acid Res Mol Biol 54*:293–332.

DeRiemer LH, Meares CF, Goodwin DA, Diamanti CJ. 1981. BLEDTA II: Synthesis of a new tumor-visualizing derivative of Co(III)-Bleomycin. *J Labelled Compd Radiopharmaceut 18*:1517–1534.

Easterwood TR, Major F, Malhotra A, Harvey SC. 1994. Orientations of transfer RNA in the ribosomal A and P-sites. *Nucleic Acids Res 22*:3779–3786.

England TE, Bruce AG, Uhlenbeck OC. 1980. Specific labeling of 3′ termini of RNA with T4 RNA ligase. *Methods Enzymol 65*: 65–74.

Fairclough RH, Cantor CR. 1979a. The distance between the anticodon loops of two tRNAs bound to the 70 S *Escherichia coli* ribosome. *J Mol Biol 132*:575–586.

Fairclough RH, Cantor CR. 1979b. An energy transfer equilibrium between two identical copies of a ribosome-bound fluorescent transfer RNA analogue: Implications for the possible structure of codon-anticodon complexes. *J Mol Biol 132*:587–601.

Fuller W, Hodgson A. 1967. Conformation of the anticodon loop in tRNA. *Nature 215*:817–821.

Girshovich AS, Bochkareva ES, Vasiliev VD. 1986. Localization of elongation factor Tu on the ribosome. *FEBS Lett 197*:192–198.

Gornicki P, Nurse K, Hellmann W, Boublik M, Ofengand J. 1984. High resolution localization of the tRNA anticodon interaction site on the *Escherichia coli* 30 S ribosomal subunit. *J Biol Chem 259*: 10493–10498.

Grajevskaja RA, Ivanov YV, Saminsky EM. 1982. 70-S ribosomes of *Escherichia coli* have an additional site for deacylated tRNA binding. *Eur J Biochem 128*:47–52.

Green R, Noller HF. 1997. Ribosomes and translation. *Annu Rev Biochem 66*:679–716.

Hüttenhofer A, Noller HF. 1992. Hydroxyl radical cleavage of tRNA in the ribosomal P-site. *Proc Natl Acad Sci USA 89*:7851–7855.

Hüttenhofer A, Noller HF. 1994. Footprinting mRNA-ribosome complexes with chemical probes. *EMBO J 13*:3892–3901.

Johnson AE, Adkins HJ, Matthews EA, Cantor CR. 1982. Distance moved by transfer RNA during translocation from the A-site to the P-site on the ribosome. *J Mol Biol 156*:113–140.

Joseph S, Noller HF. 1996. Mapping the rRNA neighborhood of the acceptor end of tRNA in the ribosome. *EMBO J 15*:910–916.

Joseph S, Weiser B, Noller HF. 1997. Mapping the inside of the ribosome with an RNA helical ruler. *Science 278*:1093–1098.

Kaziro Y. 1978. The role of guanosine 5′-triphosphate in polypeptide chain elongation. *Biochim Biophys Acta 505*:95–127.

Kim SH, Quigley GH, Suddath FL, McPherson A, Sneden D, Kim JJ, Weinzierl J, Rich A. 1973. Three-dimensional structure of yeast phenylalanine transfer RNA: Folding of the polynucleotide chain. *Science 179*:285–288.

Kirillov SV, Makarov EM, Semenkov YP. 1983. Quantitative study of interaction of deacylated tRNA with *Escherichia coli* ribosomes. Role of 50 S subunits in formation of the E site. *FEBS Lett 157*:91–94.

Lake JA. 1977. Aminoacyl-tRNA binding at the recognition site is the first step of the elongation cycle of protein synthesis. *Proc Natl Acad Sci USA 74*:1903–1907.

Lake JA. 1980. Ribosome structure and functional sites. In: Chambliss G, Craven GR, Davies J, Davis K, Kahan L, Nomura M, eds. *Ribosomes: Structure, function, and genetics*. Baltimore, Maryland: University Park Press. pp 207–236.

Lill R, Lepier A, Schwagele F, Sprinzl M, Vogt H, Wintermeyer W. 1988. Specific recognition of the 3′-terminal adenosine of tRNAPhe in the exit site of *Escherichia coli* ribosomes. *J Mol Biol 203*:699–705.

Lill R, Robertson JM, Wintermeyer W. 1984. tRNA binding sites of ribosomes from *Escherichia coli. Biochemistry 23*:6710–6717.

Lim V, Venclovas C, Spirin A, Brimacombe R, Mitchell P, Mueller F. 1992. How are tRNAs and mRNA arranged in the ribosome? An attempt to correlate the stereochemistry of the tRNA-mRNA interaction with constraints imposed by the ribosomal topography. *Nucleic Acids Res 20*:2627–2637.

Major F, Turcott M, Gautheret D, Lapalme G, Fillion E, Cedergren R. 1991. The combination of symbolic and numerical computation for three-dimensional modeling of RNA. *Science 253*:1255–1260.

Malhotra A, Penczek P, Agrawal RK, Gabashvili IS, Grassucci RA, Junemann R, Burkhardt N, Nierhaus KH, Frank, J. 1998. *Escherichia coli* 70S ribosome at 15 Å resolution by cryo-electron microscopy: Localization of fMet-tRNA$_f^{Met}$ and fitting of L1 protein. *J Mol Biol 280*:103–116.

Matzke AJ, Barta A, Kuechler E. 1980. Mechanism of translocation: Relative arrangement of tRNA and mRNA on the ribosome. *Proc Natl Acad Sci USA 77*:5110–5114.

McDonald JJ, Rein R. 1987. A stereochemical model of the transpeptidation complex. *J Biomol Struc Dyn 4*:729–744.

Moazed D, Noller HF. 1989. Intermediate states in the movement of transfer RNA in the ribosome. *Nature 342*:142–148.

More JJ, Wu ZJ. 1997. Global continuation for distance geometry problems. *J Optim 7*:814–836.

Mueller F, Stark H, van Heel M, Rinke-Appel J, Brimacombe R. 1997. A new model for the three-dimensional folding of *Escherichia coli* 16S ribosomal RNA. III. The topography of the functional centre. *J Mol Biol 271*:566–587.

Nagano K, Nagano N. 1997. Transfer RNA docking pair model in the ribosomal pre- and post-translocational states. *Nucleic Acids Res 25*:1254–1264.

Nagano K, Takagi H, Harel M. 1991. The side-by-side model of two tRNA molecules allowing the a-helical conformation of the nascent polypeptide during the ribosomal transpeptidation. *Biochimie 73*:947–960.

Nierhaus KH, Wadzack J, Burkhardt N, Junemann R, Meerwinck W, Willumeit R, Stuhrmann HB. 1998. Structure of the elongating ribosome: Arrangement of the two tRNAs before and after translocation. *Proc Natl Acad Sci USA 95*:945–950.

Nissen P, Kjeldgaard M, Thirup S, Polekhina G, Reshetnikova L, Clark BFC, Nyborg J. 1995. Crystal structure of the ternary complex of Phe-tRNA^{Phe}, EF-Tu, and a GTP analog. *Science 270*: 1464–1472.

Noller HF, Moazed D, Stern S, Powers T, Allen PN, Robertson JM, Weiser B, Triman K. 1990. Structure of rRNA and its functional interactions in translation. In: Hill WE, Dahlberg A, Garrett RA, Moore PB, Schlessinger D, Warner JR, eds. *The ribosome: Structure, function, and evolution*. Washington, DC: American Society of Microbiology. pp 73–92.

Ofengand J. 1980. The topography of tRNA binding sites on the ribosome. In: Chambliss G, Craven GR, Davies J, Davis K, Kahan L, Nomura M, eds. *Ribosomes: Structure, function, and genetics.* Baltimore, Maryland: University Park Press. pp 497–520.

Ofengand J, Ciesiolka J, Denman R, Nurse K. 1986. Structural and functional interactions of the tRNA-ribosome complex. In: Hardesty B, Kramer G, eds. *Structure, function, and genetics of ribosomes*. New York: Springer-Verlag.

Ofengand J, Lin FL, Hsu L, Boublik M. 1981. Three-dimensional arrangement of tRNA at the donor and acceptor sites of the *E. coli* ribosome. In: Siddiqui MA, Krauskopf M, Weissbach H, eds. *Molecular approaches to gene expression and protein structure.* New York: Academic Press, Inc. pp 1–31.

Olson HM, Grant PG, Cooperman BS, Glitz DG. 1982. Immunoelectron microscopic localization of puromycin binding on the large subunit of the *Escherichia coli* ribosome. *J Biol Chem 257*:2649–2656.

Paulsen H, Robertson JM, Wintermeyer W. 1983. Topological arrangement of two transfer RNAs on the ribosome. Fluorescence energy transfer measurements between A and P-site-bound tRNA^{phe}. *J Mol Biol 167*:411–426.

Prabahakaran M, Harvey SC. 1989. Models for two tRNAs bound to successive codons on mRNA on the ribosome. *J Biomol Struc Dyn 7*:167–179.

Rana TM, Meares CF. 1990. Specific cleavage of a protein by an attached iron chelate. *J Am Chem Soc 112*:2457–2458.

Rheinberger HJ, Sternbach H, Nierhaus KH. 1981. Three tRNA binding sites on *Escherichia coli* ribosomes. *Proc Natl Acad Sci USA 78*:5310–5314.

Rich A. 1974. How transfer RNA may move inside the ribosome. In: Nomura M, Tissieres A, Lengyel P, eds. *Ribosomes*. Cold Spring Harbor, New York: Cold Spring Harbor Laboratory Press. pp 871–884.

Rould MA, Perona JJ, Soll D, Steitz TA. 1989. Structure of *E. coli* glutaminyl-tRNA synthetase complexed with tRNA^{Gln} and ATP at 2.8 Å resolution. *Science 246*:1135–1142.

Ruff M, Krishnaswamy S, Boeglin M, Poterszman A, Mitschler A, Podjarny A, Rees B, Thierry JC, Moras D. 1991. Class II aminoacyl transfer RNA synthetases: Crystal structure of Yeast aspartyl-tRNA synthetase complexed with tRNA^{Asp}. *Science 252*: 1682–1689.

Samaha RR, Green R, Noller HF. 1995. A base pair between tRNA

and 23S rRNA in the peptidyl transferase centre of the ribosome. *Nature 377*:309–314.
Sampson JR, DiRenzo AB, Behlen LS, Uhlenbeck OC. 1989. Nucleotides in yeast $tRNA^{Phe}$ required for the specific recognition by its cognate synthetase. *Science 243*:1363–1366.
Smith D, Yarus M. 1989. tRNA–tRNA interactions within cellular ribosomes. *Proc Natl Acad Sci USA 86*:4397–4401.
Spirin AS. 1983. Location of tRNA on the ribosome. *FEBS Lett 156*:217–221.
Spirin AS. 1985. Ribosomal translocation: Facts and models. *Prog Nucleic Acid Res Mol Biol 32*:75–114.
Spirin AS, Lim V. 1986. Stereochemical analysis of ribosomal transpeptidation, translocation, and nascent peptide folding. In: Hardesty B, Kramer G, eds. *Structure, function, and genetics of ribosomes*. New York: Springer-Verlag.
Spirin AS, Lim VI, Brimacombe R. 1993. The arrangement of tRNA in the ribosome. In: Nierhaus KH, Franceschi F, Subramanian AR, Erdmann VA, Wittmann-Liebold B, eds. *The translational apparatus: Structure, function, regulation, evolution*. New York: Plenum Press.
Stark H, Orlova EV, Rinke-Appel J, Junke N, Mueller F, Rodnina M, Wintermeyer W, Brimacombe R, van Heel M. 1997a. Arrangement of tRNAs in pre- and posttranslocational ribosomes revealed by electron cryomicroscopy. *Cell 88*:19–28.
Stark H, Rodnina MV, Rinke-Appel J, Brimacombe R, Wintermeyer W, van Heel M. 1997b. Visualization of elongation factor Tu on the *Escherichia coli* ribosome. *Nature 389*:403–406.
Stern S, Weiser B, Noller HF. 1988. Model for the three-dimensional folding of 16 S ribosomal RNA. *J Mol Biol 204*:447–481.
Sundaralingam M, Brennan T, Yathindra N, Ichikawa T. 1975. Stereochemistry of messenger RNA (codon)-transfer RNA (anticodon) interaction on the ribosome during peptide bond formation. In: Sundaralingam M, Rao ST, eds. *Structure and conformation of nucleic acids and protein-nucleic interactions*. Baltimore, Maryland: University Park Press. pp 101–115.
Wagenknecht T, Carazo JM, Radermacher M, Frank J. 1989. Three-dimensional reconstruction of the ribosome from *Escherichia coli*. *Biophys J 55*:455–464.
Wells BD, Cantor CR. 1980. Ribosome binding by tRNAs with fluorescent labeled 3′ termini. *Nucleic Acids Res 8*:3229–3246.
Westhof E, Dumas P, Moras D. 1988. Restrained refinement of two crystalline forms of yeast aspartic acid and phenylalanine transfer RNA crystals. *Acta Crystallogr A 44*:112–123.
Wilson KS, Noller HF. 1998. Molecular movement inside the translational engine. *Cell 92*:337–349.
Woese C. 1970. Molecular mechanics of translation: A reciprocating ratchet mechanism. *Nature 226*:817–820.
Wower J, Hixson SS, Zimmermann RA. 1989. Labeling the peptidyltransferase center of the *Escherichia coli* ribosome with photoreactive tRNA(Phe) derivatives containing azidoadenosine at the 3′ end of the acceptor arm: A model of the tRNA-ribosome complex. *Proc Natl Acad Sci USA 86*:5232–5236.
Wower J, Sylvers LA, Rosen KV, Hixson SS, Zimmermann. 1993. A model of the tRNA binding sites on the *Escherichia coli* ribosome. In: Nierhaus KH, Franceschi F, Subramanian AR, Erdmann VA, Wittmann-Liebold B, eds. *The translational apparatus: Structure, function, regulation, evolution*. New York: Plenum Press. pp 455–464.